Available online at www.sciencedirect.com
SCIENCE DIRECT®
International Journal of Heat and Mass Transfer 48 (2005) 3817–3832
International Journal of HEAT and MASS TRANSFER
www.elsevier.com/locate/ijhmt

Design of a novel, intensified heat exchanger for reduced fouling rates

D. Bouris [a,*], E. Konstantinidis [a], S. Balabani [b], D. Castiglia [b], G. Bergeles [c]

[a] *Department of Engineering and Management of Energy Resources, University of Western Macedonia, Kastorias & Fleming, 50100 Kozani, Greece*

[b] *Department of Mechanical Engineering, King's College London, Strand WC2R, 2LS, UK*

[c] *Laboratory of Aerodynamics, Department of Mechanical Engineering, National Technical University of Athens, 5 Heroon Polytechnioy, 15710 Zografou, Athens, Greece*

Received 13 September 2004
Available online 8 June 2005

Abstract

This paper describes an integrated approach into the design and evaluation of a novel tube bundle heat exchanger that achieves higher heat transfer levels at lower levels of pressure drop, while remaining less susceptible to gas-side fouling. The approach combines laboratory scale experiments with industrial observations and numerical simulations of full-scale heat exchangers to study the thermal, hydraulic and fouling characteristics of tube bundle heat exchangers. Three arrangements are compared and the advantages of the proposed novel arrangement are demonstrated. Enhanced heat transfer rates are combined with reduced pressure drop and gas-side fouling rates through careful design of the shape of the tube cross-section and reduced transverse spacing.

Keywords: Heat exchangers; Tube bundles; Fouling; Vortex shedding; Numerical simulation; Experimental measurements

1. Introduction

Tube bundle heat exchangers are encountered in many engineering applications such as the power generation industry, e.g., in lignite utility boilers, where they are used as heaters or super-heaters. Designing such a heat exchanger is a complex task, as many factors have to be considered: heat transfer rates, fouling, power consumption, flow induced noise and vibration, etc. and quite often a compromise must be made.

Two standard tube bundle arrangements are commonly employed in industry, the staggered and the in-line one with tubes of a circular cross-section. At low Reynolds numbers staggered arrangements tend to induce higher turbulence levels and offer higher heat transfer rates than in-line ones but they also exhibit higher pressure drop and therefore energy consumption. On the other hand, in-line configurations are more prone to flow-induced vibrations due to the synchronization of vortex shedding between subsequent rows [1] in comparison to the staggered ones and are also more prone to blockage due to gas-side fouling [2].

* Corresponding author. Tel.: +30 2310 991324; fax: +30 24610 21731.
E-mail addresses: dbouris@enman.auth.gr, dmpouris@uowm.gr (D. Bouris).

0017-9310/$ - see front matter © 2005 Elsevier Ltd. All rights reserved.
doi:10.1016/j.ijheatmasstransfer.2005.03.026

Nomenclature

a, b	elliptic shaped tube axes (m)
A_c, A_f	heat transfer surface area under clean and fouled conditions respectively (m^{-2})
C_D	aerodynamic resistance coefficient
C_s	coefficient of Smagorinsky sub-grid scale model
C_p	specific thermal capacity ($J\,kg^{-1}\,K^{-1}$)
d	diameter of base case tube (m)
D_h	hydraulic diameter (m)
d_x, d_y	height and rear diameter of DDEFORM tube (m)
d_p	particle diameter (m)
d^*	characteristic length for circular, elliptic and DDEFORM tubes (m)
f	frequency (Hz)
g	acceleration of gravity ($m\,s^{-2}$)
h	convection coefficient ($W\,m^{-2}\,K^{-1}$)
k	thermal conductivity of fluid ($W\,m^{-1}\,s^{-1}$)
K_{th}	thermophoresis coefficient ($kg\,m^2\,s^{-2}$)
L, W, H	length, width and height of experimental test section (m)
l_ξ, l_η	metric coefficients for orthogonal curvilinear grid
m_p	particle mass (kg)
$\dot{m}$	mass flow rate ($kg\,s^{-1}$)
Nu	Nusselt number ($= q''_w d/k(T_{wall} - T_{flow})$)
Pr	Prandtl number ($=C_p\mu/k$)
q''_w	heat flux on wall ($W\,m^{-2}$)
Q_i, Q_P, Q'_A	impact energy, plastic deformation energy, adhesion energy ($kg\,m^2\,s^{-2}$)
Q_L, Q_{lift}	elastic wave propagation energy, lift force energy ($kg\,m^2\,s^{-2}$)
Re_{dg}	Reynolds number ($=U_{gap}d\rho/\mu$)
R_{ft}, R_c	thermal resistances of fouled and clean tubes respectively ($m^2\,K\,W^{-1}$)
Stk	particle Stokes number ($=\rho_p d_p^2 U_b/18\mu d$)
St	Stanton number ($=h/\rho U_{max} C_p$)
Sth	Strouhal number ($=fd^*/U_{gap}$)
S_L, S_T	longitudinal and lateral spacing of tube centers in a tube bundle (m)
$S_{\xi\xi}$, $S_{\eta\eta}$, $S_{\xi\eta}$	rate of strain (S_{ij}) components (s^{-1})
S_Φ	source terms for Navier–Stokes equations
T	temperature (K or °C)
t	time (s)
u, U_b, U_{gap}	axial velocity, free stream bulk velocity, bundle gap velocity ($m\,s^{-1}$)
v, V_r	lateral velocity, particle rebound velocity ($m\,s^{-1}$)
$\vec{v}_g$, $\vec{v}_p$	gas and particle velocity vector ($m\,s^{-1}$)
x, y	cartesian directions
y^+	non-dimensional distance from wall

Greek symbols

Γ	diffusion coefficient ($kg\,m^{-1}\,s^{-1}$)
Δ	filter width of volume average (m)
μ_{eff}, μ, μ_t	effective, fluid and turbulent dynamic viscosity ($kg\,m^{-1}\,s^{-1}$)
ξ, η	orthogonal curvilinear co-ordinate directions
ρ, ρ_p	fluid and particle density ($kg\,m^{-3}$)

Fouling is a major and still unresolved problem in heat exchanger operation. During the design stage, gas-side fouling (i.e., fouling of the outer surface of the tubes) is accounted for by making allowance for the added thermal resistance that the deposited layers introduce to the heat transfer process. This is essentially achieved through the introduction of extra heat transfer surface in the heat exchanger. An example of such an approach is the implementation of the percentage over surface index, OS ([3])

$$\mathrm{OS} = 100 \cdot \frac{R_{ft}}{R_c} = 100 \cdot \left(\frac{A_f}{A_c} - 1 \right) \tag{1}$$

where (R_c) is the clean overall heat transfer resistance and (R_{ft}) is the total fouling resistance, basically representing the insulating effect of the deposits on the heat transfer surfaces. The heat transfer surface area under clean operating conditions is (A_c), while the required surface area under fouled conditions is (A_f). In effect, fouling is accounted for by increasing the heat transfer surface by a percentage factor of (OS) i.e., longer tubes, larger tubes or more tubes. This is a common approach, which not only affects initial capital cost directly but also operating costs since the increased surface area has an indirect effect on pressure drop and the fouling process itself. In lignite utility boilers, blockage between the tube rows is often observed due to fouling, even at increased tube spacings. Further reducing the spacing or increasing tube size to accommodate the increase in heat transfer surface will intensify the problem, necessitating more frequent maintenance and cleaning and therefore increase the operating costs. Thus, even if the extra capital cost due to the increased heat transfer area is overlooked, the actual heat transfer enhancement achieved through the OS approach is often hindered by the increase in fouling rates that also affects the overall efficiency of the system.

Other than accounting for the effects of fouling during initial design, the most common approaches to control fouling during heat exchanger operation are surface cleaning techniques, including such recent methods as sonic cleaning, and/or the use of chemical additives. Sur-

face cleaning, which is more suited to utility boiler heat exchangers, could be continuous, requiring large, expensive installations that will not interfere with the process or it could be periodic. Periodic cleaning is more common in utility boilers, but almost always requires undesirable shut-down of the process and is usually synchronised with the maintenance schedule. The observed asymptotic behaviour of deposit formation in lignite utility boilers [4] implies that heat exchangers could be operating under highly fouled conditions for a large part of the inter-maintenance period. An optimum solution would be to achieve reduction of fouling rates during the design stage of the heat exchanger, as proposed in the present study, so that cleaner operation is ensured for longer periods of time.

When dealing with the problem of fouling, low levels of pressure drop and flow induced vibrations should not be compromised. Flow induced vibrations are a major concern in the design of shell- and tube-heat exchangers, primarily in nuclear reactors but also in power plant utilities causing tube failures and increasing operating and maintenance costs even further. Cross-flow excitation mechanisms such as turbulence buffeting, vortex shedding, acoustic resonance and fluid-elastic instability have been suggested in the literature [5]. On the other hand, the pressure drop across the tube bundle puts higher demands on pumping power, and therefore energy costs. Streamlined tube shapes, such as oval ones, have been previously considered in the literature due to their smaller pumping requirements [6,7] but their fouling behaviour has not been examined.

The work presented here is a synergistic blend between experimentation, numerical simulations and industrial observations into developing a novel heat exchanger that minimises fouling while increasing the heat transfer and lowering the pressure drop. A number of in-line tube bundle heat exchanger geometries are experimentally and numerically studied in order to assess their gas-side thermal, hydraulic and fouling behaviour, while assuming that possible variations of the shape of the inner tube surfaces will not significantly affect the study. Three different tube shapes (namely circular, elliptic and drop-shaped) are considered at two transverse spacings; one of the spacings is similar to the one employed in typical industrial heat exchangers (e.g., at the lignite utility boilers of the Public Power Corporation of Greece, PPC). The design methodology followed is explained in detail and the selection of the various tube bundle arrangements described. The heat transfer, pressure drop and fouling characteristics of the various tube bundle geometries are compared by means of numerical simulations at full-scale and at the actual operating conditions of the lignite utility boilers of PPC. This is followed by lab-scale experiments and simulations to give further insight into the mechanisms responsible for the different behaviour observed. The outcome is an arrangement implementing a novel tube shape which performs favourably well in terms of particle deposition, heat transfer and pressure drop. This study is part of a long-term research programme into the effects of fouling on heat exchangers in lignite utility boilers and into alternative techniques for process intensification and fouling minimisation.

2. Description of the design approach

2.1. Design and selection of the tube bundle arrangements

The starting point in this investigation was a typical industrial heat exchanger employed by the Public Power Corporation of Greece (PPC) in its lignite utility boilers. The heat exchanger comprised an in-line tube bundle configuration. The tubes were of a circular cross-section with an outer diameter of $d = 0.038$ m and they were spaced at 2.1 and 3.6 diameters in the longitudinal and transverse direction, respectively, i.e., $S_L/d = 2.1$, $S_T/d = 3.6$ (see Fig. 1). This tube bundle heat exchanger operates at a flue gas velocity of $U_b = 10$ m/s, a flow temperature of $T = 1000$ K and a tube wall temperature of $T = 800$ K, ($Re_{dg} \approx 4300$, based on gap velocity and tube diameter).

Various design modifications were introduced to the above arrangement and tested both experimentally and numerically. The modifications involved changing the shape of the tube cross-sections from circular to a more streamlined shape in order to reduce deposition rates and pressure drop. The absolute spacings between tubes were kept the same as was the total tube surface area, in order to facilitate direct comparisons with regard to shape only. The first cross-sectional shape considered was an elliptic one with an axis ratio of 2:1 studied in detail in [8,9], while the second one was a novel tube shape, derived from numerical predictions of the gas-side deposit formation on lignite utility boiler heat exchanger tube bundles [4].

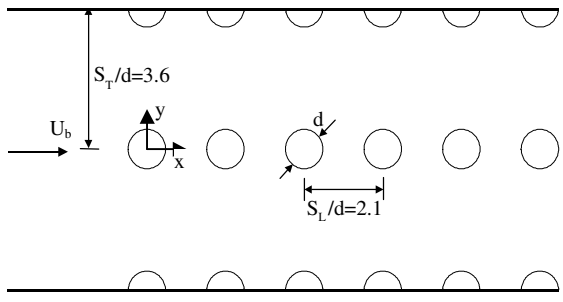

Fig. 1. Standard in-line tube bundle arrangement with circular tubes employed in lignite utility boilers of the PPC of Greece.

Fig. 2. Photograph of deposit formation in a lignite utility boiler (PPC of Greece).

The modifications were guided by the numerical prediction of deposit formation and growth, as well as industrial observations by the PPC of Greece, which showed that the asymptotic growth behaviour characteristic of heat exchanger fouling alters the original tube shape due to deposit build-up (Fig. 2). Depending on the direction of the ash particle laden flow or flue-gases, the tube surface takes on a streamlined shape. It is proposed that this might contribute to the gradual reduction of deposition rate (a characteristic of the asymptotic behaviour) along with other phenomena such as deposit removal and aging, which have been well documented in the literature [3]. Based on this assumption, the numerically calculated deposit shape was used as a guide in the design of a new tube cross-section with a parabolic upstream shape and a semi-circular one downstream. The proposed tube cross-section was termed the DDEFORM (Deposit DEtermined FOuling Reducing Morphology) tube [10].

The cross-section of the three tube shapes (namely, circular, elliptic and DDEFORM) is shown schematically in Fig. 3. The dimensions correspond to the full size utility boiler heat exchanger tubes. The effect of the tube shape on heat transfer, pressure drop and fouling was determined by numerical simulations of the particle laden gas flow in the full-scale in-line tube bundles with the spacings of the industrial heat exchangers (i.e., 2.1×3.6). Lab scale models were also tested experimentally in order to resolve the velocity characteristics and provide data for the validation of the numerical methodologies employed. Subsequently, the transverse spacing of the bundles was reduced by 50% to double the number of tube columns and subsequently the heat transfer area (Fig. 4) and the behaviour of the new closely spaced bundles with elliptic and DDEFORM tubes was studied numerically. These studies were driven by the reduced pressure drop and heat transfer rates predicted in the originally modified tube bundles, as will be shown in the following section. The geometric characteristics and the flow Reynolds numbers for the five tube bundle arrangements studied in total are summarised in Table 1. The flow passage hydraulic diameter is calculated as [3].

$$D_{\mathrm{h}} = \frac{4LA_{\min}}{A_{\mathrm{htr}}} \tag{2}$$

where L is the flow passage length, $A_{\min}$ the minimum flow passage area and A_{htr} the heat transfer surface area that corresponds to the length L. The flow passage Reynolds number is given by $Re_{D_{\mathrm{h}}} = U_{\mathrm{gap}} D_{\mathrm{h}} \rho / \mu$, with

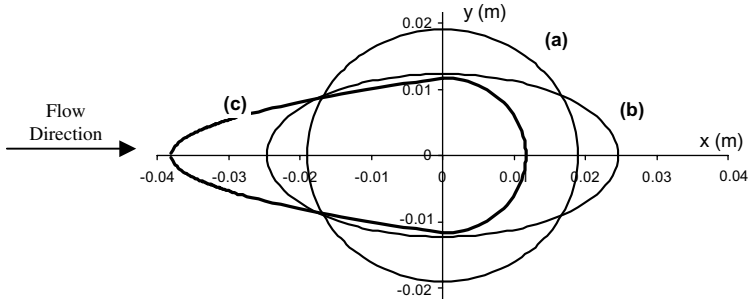

Fig. 3. Three different tube cross-sections: (a) Standard circular tube, (b) elliptic cross-section with a 2:1 axis ratio and (c) the proposed deposit determined tube shape (DDEFORM).

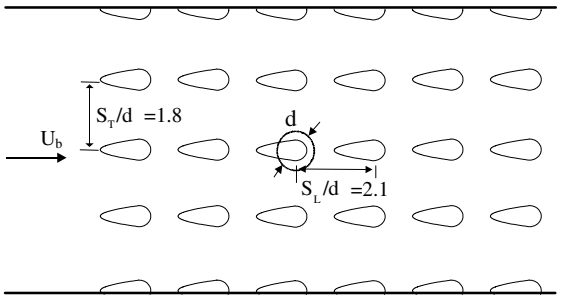

Fig. 4. In-line tube bundle arrangement with DDEFORM tubes placed at half the transverse spacing of the standard in-line arrangement.

$U_{gap} = \dot{m}/\rho A_{min}$ the gap velocity defined as the maximum average velocity, i.e., in the minimum flow passage cross-section. Streamlining the tube shape while keeping the surface area the same, results in an increase of about 14% in the flow passage hydraulic diameter for the elliptic and DDEFORM tube bundles with the large transverse spacing in comparison to the in-line tube bundle with circular tubes; a reduction of about 55% occurs when the transverse spacing is halved while the heat transfer area is doubled by accommodating more tubes. Thus, the flow passage Reynolds number reflects both changes in the tube shape and the spacing and was considered representative in the present investigation; Re_{D_h} values range from 14,000 to 30,000 and lie in the relatively low end of the sub-critical regime for all the arrangements investigated. It is interesting to note that the proposed reduced transverse spacing leads to surface to volume ratios of 10–20 (Table 1), which is far below the ratio for compact heat exchangers (chosen as an extreme) that lies in the range of 200–600 for Re_{D_h} in the order of 400–20,000 [11].

It should be noted, however, that it is normal practice in tube bundle studies to define Reynolds number based on the gap velocity and a characteristic diameter, which in the case of circular tubes is the tube diameter and for the non-circular ones the cross-flow length of the tubes (i.e., the minor axis of the elliptic tubes and the diameter of the bottom circular section of the DDEFORM tube). If this definition is employed, the Reynolds numbers in the numerical investigation and based in the actual operating conditions range from 2200 to 4100, which is still at the lower end of the sub-critical regime. Reynolds numbers based on both definitions are presented in Table 1 in order to facilitate comparison with previous studies.

Another point needs to be made here regarding the increase in surface area shown in Eq. (1) that is usually applied to account for fouling resistance. In a previous study [4], the heat transfer resistance caused by fouling for the initial 8 h under industrial operating conditions, was calculated to be an extra 0.0012–0.002 $K\,m^2/W$—depending on the material of the deposit—on top of the clean tube heat transfer resistance of ~0.009 $K\,m^2/W$. This amounts to a 20% increase in the resistance to the heat transfer process and so it would be standard practice to oversize the heat transfer surface area by such a value [12]. However, this would correspond to the deposit formation after only eight hours of operation. Considering that the numerical calculations, in agreement with industrial observations, predicted that deposit formation would reach its asymptotic state in about two weeks, a factor of 50% would be reasonable keeping in mind that values up to 100% are not uncommon as a design practice [3]. Returning to the proposed reduction in transverse spacing, it is noted that it effectively applies such an increase in heat transfer surface area. As previously mentioned, this would be expected to introduce problems related to higher pressure drop and blockage of the flow passages by the formation of deposits that bridge the spaces between neighbouring tube rows. The present study attempts to address these conflicting problems through the numerical and experimental evaluation of the proposed tube shapes and arrangements.

2.2. Numerical methodology

Most of the flows of practical interest in tube bundle arrangements are in the sub-critical regime i.e., at Reynolds numbers $10^3 < Re < 2 \times 10^5$. Numerical simulation of such flows is a complex and challenging task due to the dominant transitional effects and flow instabilities such as vortex shedding. The implemented

Table 1
Geometric characteristics and flow Reynolds numbers for the five arrangements under industrial operating conditions

	Heat transfer area/total volume ($m^2\,m^{-3}$)	Flow passage hydraulic diameter (m)	Flow passage hydraulic diameter (% std)	Flow passage Reynolds number	$Re_{dg} = \frac{U_{gap} \cdot d^*}{\nu}$
DDEFORM, $S_T/d = 1.8$	21.953	0.120	45.556	14,964	2763
Elliptic, $S_T/d = 1.8$	21.953	0.117	44.343	14,964	2992
DDEFORM, $S_T/d = 3.6$	10.976	0.302	114.747	29,927	2181
Elliptic, $S_T/d = 3.6$	10.976	0.299	113.535	29,927	2340
Circular, $S_T/d = 3.6$ (std.)	10.976	0.263	100.000	29,927	4072

methodology is a two-dimensional, time-dependent simulation using a sub-grid scale model that has been previously developed and validated [8,13]. It solves the volume averaged Navier–Stokes equations (according to Schumann [14]) on an orthogonal curvilinear grid, which have the following general conservative form:

$$\frac{\partial}{\partial t}(\rho\Phi)+\frac{1}{l_\xi l_\eta}\frac{\partial}{\partial\xi}(\rho u_\xi l_\eta\Phi)+\frac{1}{l_\xi l_\eta}\frac{\partial}{\partial\eta}(\rho v_\eta l_\xi\Phi)-\frac{1}{l_\xi l_\eta}\frac{\partial}{\partial\xi}\left(\mu_{\text{eff}}\frac{l_\eta}{l_\xi}\frac{\partial\Phi}{\partial\xi}\right)-\frac{1}{l_\xi l_\eta}\frac{\partial}{\partial\eta}\left(\mu_{\text{eff}}\frac{l_\xi}{l_\eta}\frac{\partial\Phi}{\partial\eta}\right)=S_\Phi \tag{3}$$

where l_ξ and l_η are the spatially varying metric coefficients related to the orthogonal curvilinear co-ordinates (ξ,η). $\Phi = 1$, u_ξ, v_η for the continuity, and the momentum equations respectively and S_Φ is the source term, as described in [15]. The effective viscosity is given as $\mu_{\text{eff}} = \mu + \mu_t$ where μ_t is calculated for the sub-grid scale fluctuations according to the Smagorinsky–Lilly model [16,17]:

$$\mu_t=\rho(C_s\Delta)^2|\bar{S}|=\rho(C_s\Delta)^2(2\bar{S}_{i,j}\bar{S}_{i,j})^{1/2}\quad i,j=\xi,\eta \tag{4}$$

where $\bar{S}_{\xi\xi},\bar{S}_{\xi\eta},\bar{S}_{\eta\eta}$ are the strain rate components, $\Delta = (\Delta\xi\cdot\Delta\eta)^{1/2}$ is the filter width and the constant C_s is taken to be equal to 0.1 [18,19]. The original SIMPLE algorithm [20] is combined with the Rhie and Chow modification [21] for the pressure coupling on the collocated grid. A fully implicit, first order Euler discretisation of the temporal term is used and a higher order bounded upwind scheme [22] is used for the convection terms. Periodic boundary conditions are used in the lateral direction when appropriate while the no-slip condition is applied at wall boundaries since the maximum (peak) observed y^+ value for the standard inline arrangement was much smaller ($y^+ = 3$–5) than in other cases where wall functions were used [23].

One-way coupling is considered for the particulate phase since the mass loading is only 1%. The particles are considered spherical, non-rotating and with a large enough density so that only drag, gravity and thermophoresis are considered to influence particle motion. The particle motion equation is

$$\rho_p\frac{\pi d_p^3}{6}\frac{d\vec{v}_p}{dt}=\frac{\pi}{6}d_p^3(\rho_p-\rho)\vec{g}-K_{th}\frac{\vec{\nabla}T}{T}-C_D\pi\frac{d_p^2}{8}\rho(\vec{v}_p-\vec{v}_g)\cdot|\vec{v}_p-\vec{v}_g| \tag{5}$$

where d_p is the particle diameter, v_p and v_g are the particle and carrier gas phase velocity respectively, ρ_p, ρ are the particle and gas density respectively, T is the local fluid temperature, C_D is the non-linear drag coefficient [24], and finally K_{th} is the thermophoresis coefficient [25]. Regarding the gas fluid velocity, only the contribution of the resolved field is considered as discussed in [26,8].

After particle–surface impact, adhesion or rebound is determined by an energy balance. The normal particle rebound velocity is given by

$$V_r=\left[\frac{2}{m_p}(Q_i-Q_P-Q'_A-Q_L+Q_{\text{lift}})\right]^{(1/2)} \tag{6}$$

where m_p is the particle mass. The initial kinetic energy of the particle at impact (Q_i) is lost to plastic deformation energy (Q_P) [27] and dissipated as energy due to elastic wave propagation (Q_L) [28]. The particle will rebound only if it can overcome the energy due to attractive van der Waals–London dispersion forces [29] between particle and surface (Q'_A). Hydrodynamic lift forces Q_{lift} [30] will also aid particle rebound. The tangential rebound velocity component is calculated according to [31], depending on the particle impact angle. The expressions for the energy terms in (6) are all functions of the particle and surface material properties. More details of the procedure can be found in [4,8,32].

The modelling of the particulate phase accounts for four of the five sequential events considered to take place during the fouling phenomenon: initiation, transport, attachment, removal and aging [3]. The initiation mechanism is considered by making an initial deposition rate calculation and then a subsequent one based on the previously calculated distribution of particle material on the tube surface. The solution of the flow field and particle transport equations represents the transport mechanism and the energy balance equation takes into account attachment and removal. A number of removal mechanisms that have been suggested in the literature i.e., shear, turbulent bursts [33] and erosion, as well as the aging of the deposit are not considered in the present study, but some have been modelled in previous work [4]. The present modelling approach focuses on the deposition rates and has been validated in [32] against experimentally measured particle deposition rates from the cross-flow of combustion gases around a circular cylinder.

2.3. Experimental methodology

Laboratory scale experiments were carried out in a closed circuit water facility based in ECLAT, King's College London. The facility has been used extensively for experimental heat exchanger studies and is described in detail in [9,34]. The facility delivers flow rates up to 290 l/min corresponding to bulk flow velocities of 0.93 m/s. The flow is first conditioned by passing through a hexagonal honeycomb and screens and then enters a 72 mm × 72 mm transparent working section vertically.

Three lab scale models of the heat exchanger layouts of Fig. 3 were manufactured from acrylic plastic material (Perspex) for optical access. The models comprised in-line arrangements with circular, elliptic and DDE-

FORM cylinders respectively. The diameter-to-diameter spacing between the cylinders was the same in all arrangements and similar to the one used in simulations; however, the non-dimensional spacing parameters differ as different characteristic lengths are used for the normalisation. Thus the longitudinal and transverse spacings for the arrangement with circular cylinders were $S_L/d = 2.1$ and $S_T/d = 3.6$ respectively and for the one with elliptic cylinders they were $S_L/2a = 1.6$ and $S_T/2b = 5.5$ where $2b$ and $2a$ were the minor and major axes of the elliptic cross-section of the cylinders. The arrangement with the DDEFORM cylinders had pitch ratios of $S_L/d_x = 1.6$ and $S_T/d_y = 5.8$, where d_x is the cross-sectional length in the flow direction and d_y the diameter of their circular section.

The circular cylinders had a diameter of 10 mm, the elliptic cylinders had a major axis of 13 mm and a minor axis of 6.5 mm. The DDEFORM cylinders were manufactured by joining half a cylinder of radius of 3.08 mm (bottom half) with a parabolically shaped section on the upper half.

The total cross-sectional longitudinal, d_x, and transversal lengths, d_y, of the cylinders were 13.08 and 6.16 mm respectively, the latter corresponding to the diameter of the semi-circular cylinder. The dimensions of the elliptic and DDEFORM cylinders were chosen so that the circumferential length and therefore the heat transfer area, is the same as that of the circular cylinders. Table 2 summarises the dimensions and geometrical parameters of the tube bundle models investigated.

Two of the tube columns in the test sections comprised half cylinders, which were fixed along the wall to simulate an infinite tube bundle and minimise wall boundary layer effects. The Perspex cylinders were fixed horizontally in the test section and they were rigidly mounted by pressing them tightly into holes drilled in the Perspex plates to eliminate possible resonance effects that might interfere with the flow parameters measured.

The flow structure and the velocity characteristics of the three configurations were studied by means of laser sheet flow visualisation and laser Doppler anemometry (LDA). A single component dual-beam laser Doppler anemometer (LDA) operating in forward scatter was employed which made use of a 10 mW He–Ne laser (Spectra Physics model 106). The measurement volume was 49 and 466 μm in diameter and length, respectively. Tap water was used as the working fluid and the scattered light produced by the particles in the water that crossed the measurement volume was collected by a photomultiplier. The signal produced was subsequently processed using a TSI frequency counter, model 1990B, interfaced to a PC with appropriate data acquisition software. For the flow visualisation the water was seeded with 15 μm hollow glass particles and video recordings of the flows past the tube bundles were taken.

The origin of the co-ordinate system was taken at the centre of the first row cylinder. All measurements were taken at the plane of symmetry, $z = 0.0$ mm, i.e., the plane that crosses the cylinders at midspan and in the region $0 < y/S_T < 0.5$ since the flow approaching the bundle was found to be two-dimensional and the interstitial flow was found to be symmetrical with respect to the x–y plane. The maximum uncertainty in the LDA velocity measurements was estimated to be around 5% and 10% for the mean and r.m.s. velocities respectively.

Detailed ensemble-averaged measurements of the axial and radial velocities were taken at Re of around 13,000 and 7000 for the circular and non-circular arrangements respectively. Time resolved measurements were also taken in selected locations behind each cylinder for a range of Re numbers and MATLAB software was used for power spectra estimation. It should be noted that the Re number is based on gap velocity and a characteristic length which is the cylinder diameter for the circular cylinders, the minor axis for the elliptic cylinder, $2b$, and the diameter of the bottom circular half, d_y for the DDEFORM tube.

Table 2
Dimensions and geometrical parameters of the tube bundle models

Arrangement	In-line with circular cylinders	In-line with elliptic cylinders	In-line with DDEFORM cylinders
Dimensions, $L \times W \times H$/(mm × mm × mm)	72 × 72 × 196	72 × 72 × 196	72 × 72 × 196
Cylinder diameter, d/(mm)	10		
Major axis, $2a$/(mm) or height, d_x/(mm)		13	13.08
Minor axis, $2b$/(mm) or diameter, d_y/(mm)		6.5	6.16
Transverse spacing, S_T/(mm)	36	36	36
Longitudinal spacing, S_L/(mm)	21	21	21
Transverse pitch, S_T/d, $S_T/2b$, S_T/d_y	3.6	5.5	5.8
Longitudinal pitch, S_L/d, $S_L/2a$, S_L/d_x	2.1	1.6	1.6
No. rows, N_r	6	6	6
No. columns, N_c	3	3	3
Aspect ratio, L/d, $L/2b$, L/d_y	7.2	11.08	11.7

3. Results and discussion

3.1. Numerical analysis of thermal, hydraulic and fouling behaviour

The five different tube bundle arrangements were studied using the numerical methodology previously presented. The numerical approach has been previously applied and validated against lab-scale experimental measurements and industrial observations for a number of tube bundle geometries [4,8,13,32] and therefore detailed comparison against experimental measurements is not presented here. The numerical methodology will be directly implemented as a design tool in the present study, although a comparison against experimentally measured deposition rates will be presented in Section 3.2.2 as part of the investigation of the underlying physical mechanisms. The number of grid nodes for the $S_T/d = 3.6$ transverse spacing was ~90,000 for the circular and elliptic shaped tubes and 150,000 for the DDEFORM tubes, while for the $S_T/d = 1.8$ transverse spacing the arrangement with elliptic shaped tubes had 130,000 grid nodes and the DDEFORM tube arrangement had 215,000 grid nodes. The time step for the flow calculation was 1.2×10^{-4} s and periodic conditions independent of the initial flow field were identified through monitoring of flow variables at specific positions until their mean values were unchanging. 360,000 particles were then injected over a total of 150 time steps, corresponding to one time period of the main vortex shedding motion, as calculated from the numerical simulation. Particle distribution and properties corresponded to observations during the operation of lignite utility boilers of the Public Power Corporation of Greece. The particle diameter range was 23–850 μm with the following mass distribution: 23, 68 μm : 36.7%, 118, 173 μm : 27.2%, 250, 350 μm : 23.3%, 550, 850 μm : 12.8%. Particle density was 2300 kg/s and material properties (Poisson ratio, Young's modulus etc.) were taken to be those of Al_2O_3. The corresponding Stokes numbers range from 0.42 to 573 indicating a clear inertial deposition regime for all but the smallest particles, which were at the lower limit $Stk > 0.125$. Mean values of particulate phase behaviour were obtained by averaging over the 150 time steps of their injection.

Fig. 5 compares the predicted mean Nusselt number values for the various arrangements and tube shapes as well as the heat transfer parameter $St \cdot Pr^{2/3}$ often used to characterize heat transfer in heat exchangers where St is the Stanton and Pr the Prandtl number. The dimensionless numbers, Nu, St and Pr are defined as follows:

$$St = \frac{h}{\rho U_{\text{gap}} C_p}, \quad Pr = \frac{C_p \mu}{k}, \quad Nu = \frac{hd}{k} \tag{7}$$

The comparison is made against the values of $Nu = 33.6$ and $St \cdot Pr^{2/3} = 8.67 \times 10^{-3}$ for the 'standard' in-line tube bundle with circular cross-section tubes at spacings of $S_L/d = 2.1$, $S_T/d = 3.6$. Thus, the y-axis in Fig. 5 shows a percentage value that indicates the ratio of the predicted Nu or $St \cdot Pr^{2/3}$ values for the non-circular tube bundle arrangements over the above mentioned values of the standard configuration. Using the same definitions, empirically estimated regions of Nu and $St \cdot Pr^{2/3}$ values [2,11] are also plotted in the same figure for comparison. The Nu values were obtained by using empirical relations for heat transfer from smooth in-line tube bundles [2] for the transitional and lower sub-critical Reynolds number regime, i.e., $10^2 < Re_{D_h} < 10^3$ and $10^3 < Re_{D_h} < 2 \times 10^5$, as the operating conditions under study are very close to the limit. The $St \cdot Pr^{2/3}$ values for compact heat exchangers have been calculated for similar Reynolds numbers from relevant empirical correlations found in [11], which are commonly used in compact tube bundles due to the dominance of the forced convection effects. Despite the larger scale of the present configurations, an indicative comparison with compact heat exchangers is made on the basis of the presently proposed reduction in tube spacing and size, which is characteristic of compact heat exchangers.

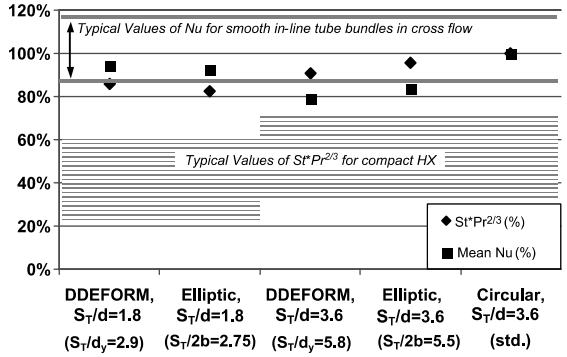

Fig. 5. Comparison of numerically calculated mean Nusselt numbers and heat transfer factors ($St \cdot Pr^{2/3}$) for the five arrangements studied. Values for the in-line circular tube arrangement with $S_L/d = 2.1$, $S_T/d = 3.6$ are: $Nu = 33.6$, $St \cdot Pr^{2/3} = 8.67 \times 10^{-3}$.

It can be seen from Fig. 5 that reducing the transverse spacing reduces the mean tube heat transfer rate more for the elliptic tubes than for the DDEFORM tubes. Furthermore the $StPr$ parameter and the mean Nusselt numbers vary within 20% between the five arrangements, and they are at the lower limit of the smooth in-line tube bundle regime and a little higher than the upper limit of the compact heat exchanger regime. However, this is not representative of the overall heat transfer rate achieved within the same volume for each heat exchanger since reducing the transverse spacing and inserting more tube rows leads to an increase in surface area. This can be accommodated through the following relation:

$$\frac{q^{\mathrm{DDEFORM}}_{S_T/d=1.8}}{q^{\mathrm{in-line(std.)}}_{S_T/d=3.6}} = \frac{\sum_{\mathrm{row}=1}^{6}\overline{Nu}^{\mathrm{row}}_{S_T/d=1.8}\cdot k\cdot\Delta T\cdot 2\cdot \mathrm{Area}^{\mathrm{row}}_{S_T/d=3.6}}{\sum_{\mathrm{row}=1}^{6}\overline{Nu}^{\mathrm{row}}_{S_T/d=3.6}\cdot k\cdot\Delta T\cdot \mathrm{Area}^{\mathrm{row}}_{S_T/d=3.6}} = \frac{\sum_{\mathrm{row}=1}^{6}\overline{Nu}^{\mathrm{row}}_{S_T/d=1.8}\cdot 2}{\sum_{\mathrm{row}=1}^{6}\overline{Nu}^{\mathrm{row}}_{S_T/d=3.6}} \quad (8)$$

where ΔT is the temperature difference between the incoming flow and the tube walls.

By applying this formula to all the arrangements studied, direct comparisons can be made as shown in Fig. 6. Changing the tube shape from circular to a more streamlined one results in a reduction in heat transfer; however, when the transverse spacing is reduced, the heat transfer increases by about 85% in both the elliptic and the DDEFORM tubes due to the increase in heat transfer area. Apparently, this increase does not imply a similar increase in actual efficiency due to adverse effects on pressure drop and fouling rates. The effect of the reduced spacing, as well as of the different tube shapes on pressure drop through the 6 tube rows is presented in Fig. 7. If the original spacing is retained, the pressure drop decreases by 85% and 81% respectively in the DDEFORM and the elliptic tube shapes. This can largely be attributed to the increase in flow passage area, as well as to the reduction in vortex shedding and flapping activity arising from the more streamlined shapes. However, even when the transverse spacing is reduced in order to increase the heat transfer area and subsequently the heat transfer rates, a significant reduction of the order of 40% is still achieved for the pressure drop, compared to that of the standard circular in-line array.

As previously mentioned, the common problem with reducing the transverse spacing in order to increase heat transfer surface area is that the flow passage area also decreases resulting in increased pressure drop and blockage of the heat exchanger due to deposit build up between the closely spaced tube rows. Fig. 8 shows how the five tube bundle arrangements numerically investigated perform in terms of deposition rate and deposition rate distribution between the tube rows. Comparing the arrangements at the larger transverse spacing, it is evident that the streamlined tube shapes of the elliptic and the DDEFORM tubes lead to a reduction in the overall deposition rate, which is most evident in the downstream tube rows, although even the first row shows a reduction in the order of 30–50%. However, as shown previously, at the large transverse spacing the benefits with regards to both heat transfer rate and pressure drop are not favourable. On the other hand, by looking at the closely spaced arrays, it can be seen that the deposition rates are still at 26% and 44% of those of the standard arrangement with circular cross-sectional tubes but heat transfer is significantly higher (see Fig. 6) and pressure drop lower (see Fig. 7). The DDEFORM tube shows a superior performance over the elliptic one in terms of deposition rates. The different behaviour of the bundles with non-circular tubes is further explored in the next section.

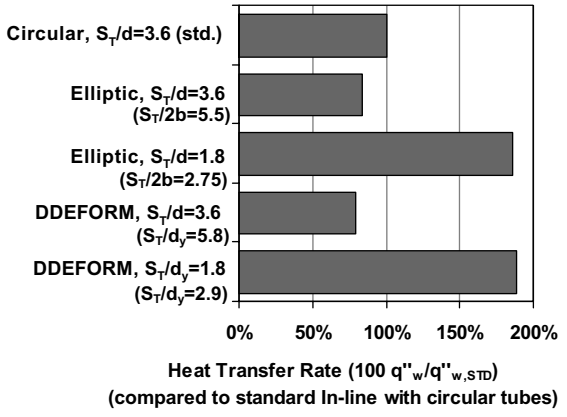

Fig. 6. Comparison of the numerically calculated overall heat transfer rates for the five arrangements studied.

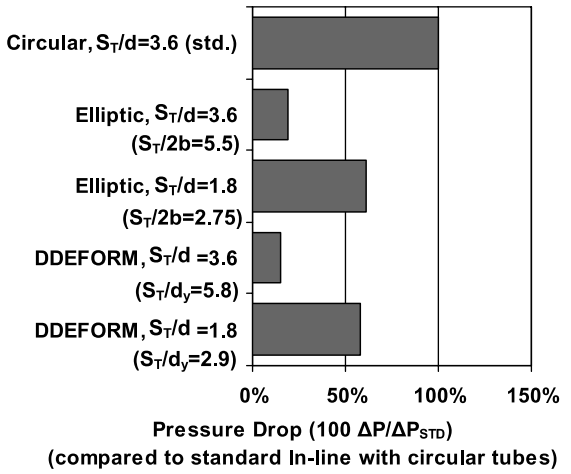

Fig. 7. Comparison of the numerically calculated overall pressure drop through the tube bundle for the five arrangements studied.

3.2. Investigation of underlying mechanisms

3.2.1. Experimental study of flow field

The interstitial flow of the three tube bundle models at the larger spacing (circular tubes, elliptic tubes and DDEFORM) was fully characterized by ensemble—averaged LDA measurements. A detailed description of the flows for each tube bundle can be found in [9,35–37] and is beyond the scope of this paper. This paper concentrates on comparisons between the bundles and more specifically on features that are important in explaining the different performance of the three tube

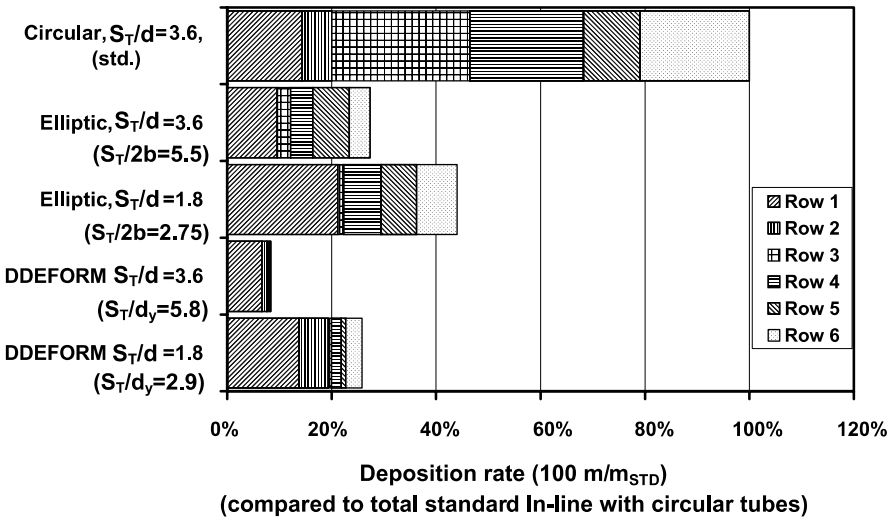

Fig. 8. Comparison of the numerically calculated deposition rates for each tube row of the five arrangements that were studied.

bundles observed by the numerical study. In order to facilitate comparisons between the different geometries the data are presented in a non-dimensional form. Thus velocities have been normalized with the bulk velocity of the approaching flow, U_b, axial measurement locations have been normalized with the longitudinal spacing S_L and the transverse ones with a characteristic diameter d^* which is equal to d for the circular tubes, $2b$ for the elliptic ones and d_y for the DDEFORM tubes.

Although the heat transfer area of the tubes and the tube layout were kept the same the different tube shapes employed altered the wake and vortex dynamics of the flows. In order to compare the velocity characteristics of the bundles under investigation axial mean velocity profiles obtained in the mid gap between successive tube rows were plotted together as shown in Fig. 9.

Fig. 9 shows that the velocity profiles for all three tube bundles change from a U-shape with steep gradients at the shear layers to a more flat distribution in the downstream rows as a result of higher velocity fluctuations in inner rows which cause better flow mixing even across the wakes. The mean velocities approach the same levels of magnitude in the free stream for all three tube bundles but the distributions differ in the wake region and shear layers particularly behind the first row. The mean velocity profiles are similar for all tube bundles behind the fourth row.

The distinctly different profiles observed behind the first row reflect the influence of tube shape on the wake structure. The three tubes exhibit different degrees of 'bluffness' and this affects the base pressure coefficient and the vortex formation length; as a result the aspect ratio of the wake is altered; thus, a streamlined body such as the elliptic cylinder with decreased bluffness compared to a circular cylinder is expected to have a longer and narrower wake bubble. In a tube bundle this is expected to be evident mainly behind the first row, which resembles the case of a single bluff body in cross-flow rather than in inner rows which are exposed to a non-uniform flow. The influence of tube shape is also demonstrated in the different vortex shedding frequencies measured in the three tube bundles as will be discussed later.

Changing the shape of the cylinders from circular to elliptic or DDEFORM does not present any advantage in terms of turbulence generation. Fig. 10 compares the magnitude of the fluctuating velocities measured at the midgap between successive rows and at the edge of the shear layers separating from the cylinders as a function of row depth in the three tube bundles. It should be noted that these values contain contributions from both random turbulence and mean flow variations due to periodic vortex shedding. The figures illustrate clearly that the fluctuation levels are considerably higher for the in-line bundle with circular tubes than with the elliptic or DDEFORM ones. Towards the exit of the bundle fluctuations build up to the saturation level [35] and the axial rms velocities attain similar values for all three tube shapes. Therefore, the effects of the different tube shape might be expected to be limited to the first rows only. Note that the influence of Reynolds number (or flow velocity) should be taken into account, since low fluctuation levels are also found in the first rows with the circular tubes at lower flow velocities [35]. The fluctuation levels for the elliptic and DDEFORM tubes are similar and vary less from row to row (especially the radial component) than the fluctuations for the circular tubes, which grow much faster. The results of the present study are in agreement with studies of single elliptic cylinders in cross-flow [38] in which the Reynolds stres-

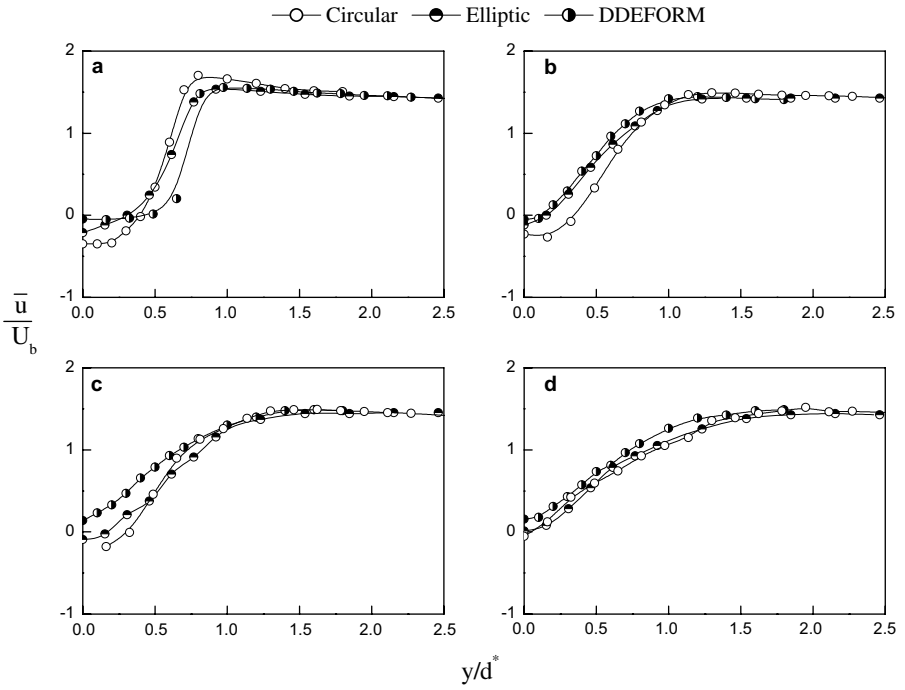

Fig. 9. Experimentally measured mean velocity profiles at mid gap between the tube rows: (a) first row; (b) second; (c) third and (d) fourth row respectively.

ses were found to be qualitatively the same as those in circular cylinders but their peak values were half in magnitude.

The lower fluctuating levels observed with elliptic and DDEFORM tubes compared to circular ones reflect the strength of the vortex shedding activity in the bundles as higher fluctuating levels in the shear layers indicate more intense vortex activity. The streamlined shape of the tubes results in weak interaction between the free stream with the wakes through the process of vortex shedding; subsequently lateral mixing is poor and heat transfer and fouling rates will be lower as found by the numerical study.

Velocity spectra were estimated for these two configurations and showed that the vortex shedding from the first and second row was suppressed due to reattachment of the separated shear layer on the downstream tubes. This was also evident downstream of the first row in the array with circular tubes [35]. These findings were confirmed by the flow visualization study, which showed that although there are vortices formed downstream of the first two rows (or only the first row for the standard array) there is not a clear frequency associated with it.

In downstream rows, the flow fluctuations associated with formation and shedding of coherent vortices in the gaps between tubes give rise to distinct peaks in the velocity spectra with different characteristics in each bundle. The spectral peaks appear at frequencies which correspond to a constant Strouhal number, $Sth = fd^*Ug$, where f is the frequency of spectral peak, for each tube bundle; Sth are equal to 0.11, 0.14 and 0.16 for the bundles with elliptic, circular and DDEFORM tubes, respectively. It is reasonable to expect a lower shedding frequency for the bundle with elliptic tubes as the base of the tube extends into its wake, thus interfering or weakening the vortex formation, particularly in the early stages of vortex growth which results in a low frequency and correspondingly low-amplitude and dispersed spectral peaks as has been observed. An elliptic cylinder also resembles a bluff body with an afterbody of a length equal to the cross-flow dimension; the Strouhal number for such bodies decreases as the afterbody length increases [39]. The finding of the spectral analysis that the Sth value for the DDEFORM tubes is higher than that for elliptic or even circular is remarkable; it reveals a pronounced effect of the forebody shape of the tubes on the flow characteristics in bundle configurations. It should be noted that a Sth number close to that measured with circular tubes is to be expected since the afterbody shape is similar for circular and DDEFORM tubes. However, the spectral peaks observed in the DDEFORM bundle are much less well-defined and do not reach the magnitude of those observed with circular tubes. The forebody of downstream tubes hinders the vortex shedding activity in the wake of the upstream tube but does not appear to alter its frequency. The

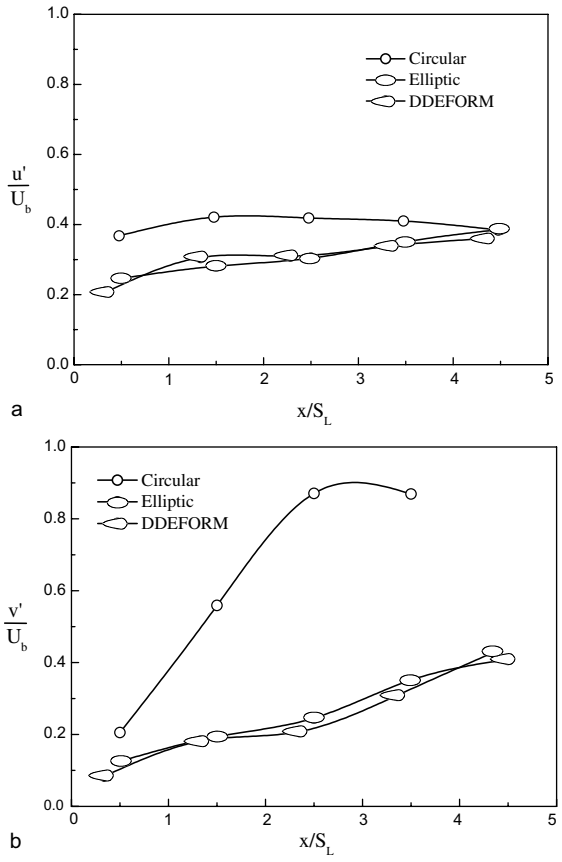

Fig. 10. Development of fluctuating velocity magnitude with row depth for different tube shapes. Measurements taken in the mid gap between successive rows and in the edge of the separating shear layers.

weak flow activity is evident also from the fluctuation levels in the gap between subsequent tubes shown in Fig. 10(b) (transverse component). The unique characteristics of the DDEFORM bundle combining a streamlined shape with low resistance to the flow and a relatively high vortex shedding frequency provide a plausible explanation for the different deposition rates found in the numerical study.

The flow visualisation study showed the typical alternate vortex shedding pattern inside the bundles with exception of the first row (and the second for the non-circular tubes). Fig. 11 shows images of the flow pattern observed behind the first and third row in the bundle with DDEFORM tubes. Flow visualization images for the other tube bundles can be found in [35,9]. The flow behind the first DDEFORM tube row is characterized by a stagnant region and the reattachment of the separated shear layer on the second row; some small vortices are also formed near the tip of the second row tube but no clear vortex shedding activity could be detected. On the contrary, the flow pattern behind the third row exhibited clear periodic vortex shedding activity.

3.2.2. Numerical and experimental study of deposition rate

The mechanism behind the improved deposition rate behaviour of the DDEFORM tube shape was numerically and experimentally investigated. Particle deposition studies were performed by Tochon and Grillot [40] using lab scale models of Perspex tubes and glass particles of 8–20 μm in diameter. Experiments were performed for each particle size class separately and a laser counter was used to measure the collection efficiencies upstream and downstream of two in-line arrangements of six tube rows, one with circular tubes and one with the DDEFORM tubes. Both arrangements were at the standard tube spacing used by the PPC of Greece while the Reynolds number, based on upstream velocity and standard tube diameter was 5700. The Stokes number of the particles ranged from 0.01 to 1, thus including the inertial deposition regime which begins at $Stk = 0.125$. In the experiments, the tubes were covered with grease so that all the particles impacting on the tubes would stick. Although this might sound unrealistic it

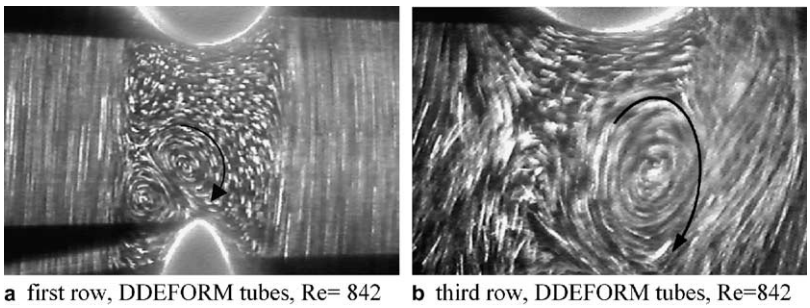

Fig. 11. Visualisation pictures acquired behind the first and third rows of the bundles with DDEFORM tubes. Flow direction is from top to bottom.

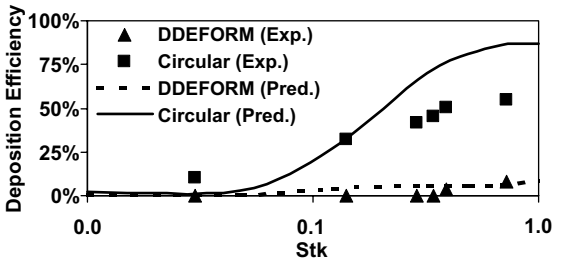

Fig. 12. Numerical calculation and experimental measurement of deposition efficiency as a function of particle Stokes number for in line bundles of tubes with circular and DDEFORM cross-sections.

was found to be the case for these particle sizes in the numerical studies [8] and therefore direct comparisons between experiments and simulations can be made.

Numerical calculations were performed on an orthogonal curvilinear grid of 150,000 nodes using the same methodology as in the previous section. Results of both measured and numerically predicted collection efficiencies, based on the same operating conditions, are presented in Fig. 12 for a range of particle Stokes numbers. The marked difference in the collection efficiencies between the circular and DDEFORM tube shapes is evident. The difference increases with *Stk* number and reaches a maximum value as *Stk* approaches 1 with the DDEFORM tubes exhibiting 90% less deposition than the circular ones. This is the same value that was numerically calculated in the previous section for the actual operating conditions of the PPC tube bundle.

Experimental measurements were also performed to assess the effect of tube rows by repeating measurements while successively adding pairs of rows to the experimental setup [40]. It was found that over 40% of the deposition occurs in the first two rows and at the high Stokes number regime. Since the tubes were greased and the inertial deposition mechanism dominates at these particles sizes, this implies that over 40% of the particles impact onto the first two rows even though the frontal area of the tubes takes up a maximum of 28% of the flow passage area. This is a very high value considering that the larger particles are relatively insensitive to diffusive behaviour, which is the only possible mechanism that could account for the extra particles arriving to the surfaces of the first two rows. A possible explanation may be a non-uniformity of the particle distribution in the upstream flow. This could also explain the higher collection efficiencies predicted by the numerical model to occur throughout the bundle and not specifically in the first rows. It should be noted that the larger particles used in the experiment correspond to the Stokes numbers of the two smallest particle sizes ($Stk(23\ \mu m) = 0.42$ and $Stk(68\ \mu m) = 3.67$) used in the previously presented numerical simulations of the actual operating conditions. Thus the predicted particle sizes that actually contribute to the deposition mechanism are in accord with the experimental findings.

In order to elucidate the mechanism responsible for the significant reduction in the deposition rate for DDEFORM tubes, snapshots of the calculated particle transport through both tube bundle arrangements (i.e., circular and DDEFORM) are presented in Figs. 13 and 14 respectively for two different particle sizes together with iso-vorticity contours. Close-up views of specific regions are shown on the same figures for clarity and comparison. Upon entering the tube bundle, all particles are evenly distributed along the transverse direction. Soon after though, they encounter the fluctuating

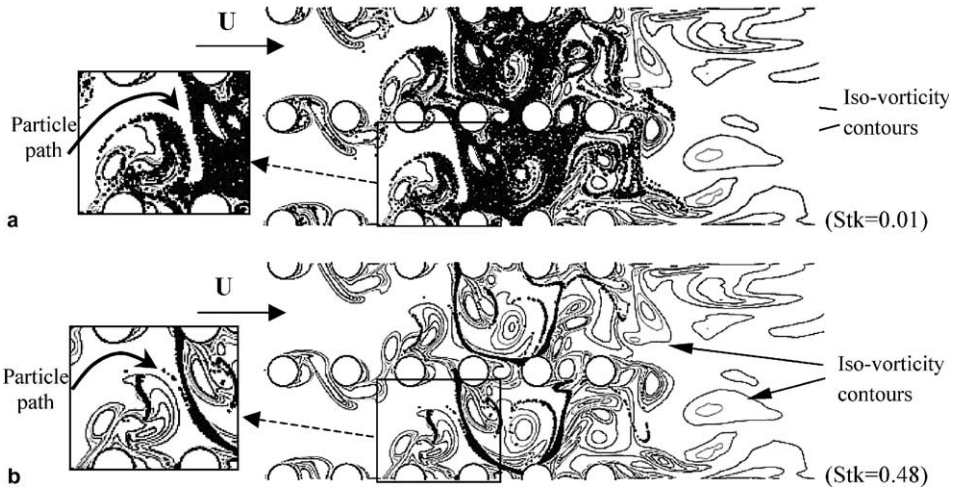

Fig. 13. Snapshot of numerically calculated particle positions and iso-vorticity contours for particle Stokes numbers (a) 0.01 and (b) 0.48 in the in-line tube bundle with circular cross-sectional tubes. Close-up views of boxed regions are shown.

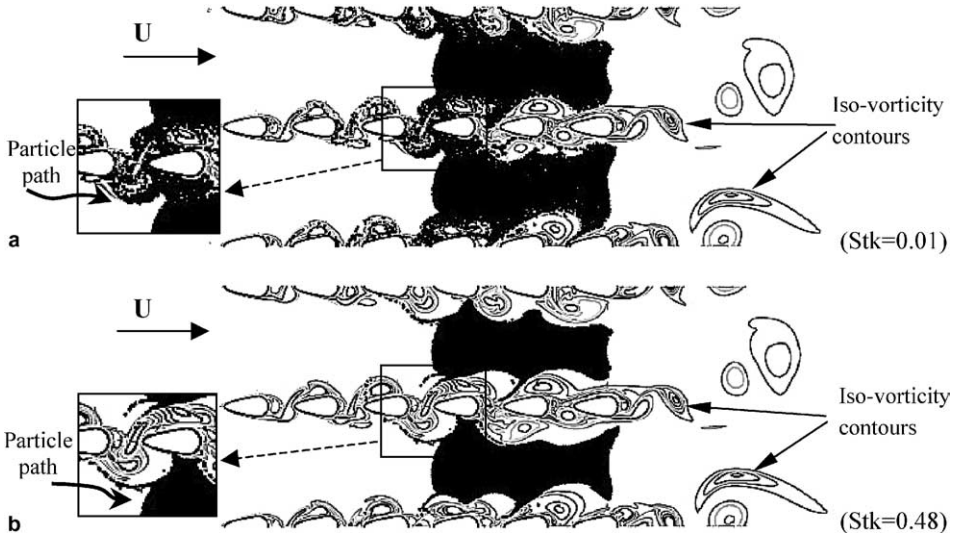

Fig. 14. Snapshot of numerically calculated particle positions and iso-vorticity contours for particle Stokes numbers (a) 0.01 and (b) 0.48 in the in-line tube bundle with DDEFORM tubes. Close-up views of boxed regions are shown.

flow field imposed by the cylinder wakes and they behave differently, depending on their size. The smallest particles with $Stk = 0.01$ (Figs. 13 and 14(a)) closely follow the flow while the larger ones with $Stk = 0.48$ (Figs. 13 and 14(b)), corresponding to the smaller particles in the industrial scale heat exchanger operating conditions, are just above the inertial deposition regime, and therefore less vulnerable to the influence of the flow pattern. It can be clearly seen that, although both particle sizes (black dots in figures) follow the vortices shed by the tubes, it is the smaller ones that are also dispersed by them and are thus more easily trapped between consecutive cylinder rows. This is particularly evident in Fig. 13 where the $Stk = 0.48$ (Fig. 13(b)) particles are concentrated along the vortex edges while the smaller particles (Fig. 13(a)) have entered into the vortex cores and have been carried into the inter-tube areas. It is suggested that this is the mechanism responsible for most of the downstream deposition and also the reason that the DDEFORM tube exhibits reduced fouling rates when placed in an in-line tube bundle arrangement. The flow passages in the arrangement with circular tubes (Fig. 13) exhibit a much higher level of mixing, and therefore turbulence levels, than the DDEFORM tubes (Fig. 14), as the experimental studies presented in the previous section have also confirmed. In regard to the difference between the DDEFORM tube and the elliptic one, it should be kept in mind that although the vortex shedding and shear layer instability phenomena are of a smaller magnitude in the DDEFORM tube arrangement, the higher shedding frequencies (see discussion in Section 3.2.1) tend to keep the suspended particles away from the streamwise inter-tube gaps, not giving them enough time to enter. Overall, this results in reduced mixing in the DDEFORM tube arrangement, minimising the interaction between particles and downstream tubes and therefore reducing deposition. Although it is well documented in the literature that reduced mixing and turbulence will adversely affect heat transfer, this can be compensated by reducing the transverse spacing and increasing the heat transfer area; the reduced deposition rate and pressure drop stemming from the streamlined shape of the DDEFORM tube allows more tubes to be fitted in the bundle optimising thus the benefits of the new tube shape.

4. Conclusions

The paper describes a design methodology for the development of an optimum heat exchanger arrangement that reduces gas-side fouling while increasing the heat transfer rate and decreasing the pressure drop. In order to address these design requirements, the approach efficiently utilized a combination of numerical CFD simulations, experiments and industrial observations of the fouling process itself in a lignite boiler heat exchanger.

Modifications of the tube shape in a typical 3.6×2.1 industrial in-line tube bundle arrangement were considered initially and thus an elliptic and a drop-shaped arrangement (DDEFORM) were examined numerically and experimentally in terms of thermal and hydraulic characteristics as well as particle deposition rates. It was found that streamlining the shape of the tubes results in 85% lower pressure drop and 90% lower deposi-

tion rates. However, the heat transfer decreased due to reduced levels of mixing and turbulence in the modified bundles and therefore a reduction in the transverse spacing was considered in order to increase the heat transfer area and maximise the benefits of the new arrangements. The study of the new closely spaced bundles showed that they attain higher heat transfer levels with a 75% lower deposition rate and 40% lower pressure drop so that the DDEFORM tube bundle design exhibits a superior performance and presents a promising technology for the reduction of fouling in heat exchangers. The underlying mechanism for the enhanced performance of this arrangement was examined in detail through simulations and experiments. Low fluctuation levels, generated inside the arrays, and particularly weak periodic activity in the wakes of the tubes are thought to be the main mechanisms reducing the particle deposition rates.

Acknowledgements

The authors are pleased to acknowledge financial support from the Commission of the European Union under contract JOU2-CT97-0064 for the work carried out for this paper. The importance of the validation using the studies performed by Drs. P. Tochon and J. M. Grillot at Greth under the above mentioned research project is also acknowledged.

References

[1] D.S. Weaver, A. Abd-Rabbo, A flow visualization study of a square array of tubes in water cross-flow, ASME J. Fluids Eng. 107 (1985) 354–363.
[2] A. Zukauskas, Convective heat transfer in crossflow, in: S. Kakac, R.K. Shah, W. Aung (Eds.), Handbook of Single-Phase Convective Heat Transfer, Wiley, New York, 1987, pp. 5.1–5.46.
[3] S. Kakac, H. Liu, Heat Exchangers, Selection, Rating and Thermal Design, CRC Press LLC, Boca Raton, FL, 1998.
[4] D. Bouris, G. Bergeles, Numerical calculation of the effect of deposit formation on heat exchanger efficiency, Int. J. Heat Mass Transfer 40 (17) (1997) 4073–4084.
[5] D.S. Weaver, J.A. Fitzpatrick, A review of cross-flow induced vibrations in heat exchanger tube arrays, J. Fluids Struct. 2 (1988) 73–93.
[6] G.P. Merker, H. Hanke, Heat transfer and pressure drop along the shell-side of tube banks having oval-shaped tubes, Int. J. Heat Mass Transfer 29 (12) (1986) 1903–1909.
[7] Q. Li, Z. Cheng, U. Flechtner, H. Warnecke, Warmeubergang und Druckverlust auf der Außenseite in flüchtend angeordneten Rohrbündeln mit ellipsoiden Rohren, Chemische Technik 49 (1997) 183–185.
[8] D. Bouris, G. Papadakis, G. Bergeles, Numerical evaluation of alternate tube bundle configurations for particle deposition rate reduction in heat exchanger tube bundles, Int. J. Heat Fluid Flow 22 (2001) 525–536.
[9] D. Castiglia, G. Papadakis, S. Balabani, M. Yianneskis, An experimental and numerical study of the flow past elliptic cylinder arrays, Proc. IMechE, Part C 215 (2001) 1287–1301.
[10] D. Bouris, G. Bergeles, Greek patent no. (I.P.O.) 100370, International Clearance: F28F 1/02, 2001.
[11] W. Kays, A. London, Compact Heat Exchangers, 3rd ed., McGraw Hill, New York, 1984.
[12] J. Chenoweth, Fouling problems in heat exchangers, in: W. Yang, Y. Mori (Eds.), Heat Transfer in High Technology and Power Engineering, Hemisphere, New York, 1987, pp. 406–419.
[13] D. Bouris, G. Bergeles, Two-dimensional time dependent simulation of the subcritical flow in a staggered tube bundle using a subgrid scale model, Int. J. Heat Fluid Flow 20 (1999) 105–114.
[14] U. Schumann, Subgrid scale model for finite difference simulations of turbulent flows in plane channels and annuli, J. Comput. Phys. 18 (1975) 376–404.
[15] F. Mouzakis, G. Bergeles, Numerical prediction of turbulent flow over a two dimensional ridge, Int. J. Numer. Methods Fluids 12 (1991) 287–296.
[16] J. Smagorinsky, General circulation experiments with the primitive equations. I. the basic experiment, Mon. Weather Rev. 91 (1963) 99–164.
[17] D. Lilly, The representation of small scale turbulence in numerical simulation experiments, in: H.H. Goldstine (Ed.), Proc. IBM Scientific Computing Symposium on Environmental Sciences, IBM Form No. 320-1951, 1967, pp. 195–210.
[18] P. Mason, N. Callen, On the magnitude of the subgrid scale eddy coefficient in large eddy simulations of turbulent channel flow, J. Fluid Mech. 162 (1986) 439–462.
[19] M. Breuer, M. Pourquie, First experiences with LES of flows past bluff bodies. in: W. Rodi, G. Bergeles (Eds.), Proc. of the third International Symposium on Engineering Turbulence Modeling and Measurements, Heraklion, Crete, Greece, 27–29 May, Elsevier, Amsterdam, 1996, pp. 177–186.
[20] S.V. Patankar, D.B. Spalding, A calculation procedure for heat, mass and momentum transfer in three dimensional parabolic flows, Int. J. Heat Mass Transfer 15 (1972) 1787.
[21] C. Rhie, W. Chow, Numerical study of the turbulent flow past an airfoil with trailing edge separation, AIAA J. 21 (1983) 1525–1532.
[22] G. Papadakis, G. Bergeles, A locally modified second order upwind scheme for convection terms discretisation, Int. J. Numer. Methods Heat Fluid Flow 5 (1995) 49–62.
[23] P. Rollet-Miet, D. Laurence, J. Ferziger, LES and RANS of turbulent flow in tube bundles, Int. J. Heat Fluid Flow 20 (1999) 241–254.
[24] R. Clift, J. Grace, M. Weber, Bubbles, Drops and Particles, Academic Press, New York, 1978.
[25] L. Talbot, R.K. Cheng, R.W. Schefer, D.R. Willis, Thermophoresis of particles in a heated boundary layer, J. Fluid Mech. 101 (4) (1980) 737–758.
[26] Q. Wang, K. Squires, Large eddy simulation of particle deposition in a vertical channel flow, Int. J. Multiphase Flow 22 (4) (1996) 667–683.
[27] S.M. Wall, W. John, S.L. Goren, Application of impact adhesion theory to particle kinetic energy loss

measurements, in: K.L. Mittal (Ed.), Particles on Surfaces, vol. 2, Plenum Press, New York, 1988.
[28] J. Reed, Energy losses due to elastic wave propagation during an elastic impact, J. Phys. D 18 (1985) 2329–2337.
[29] F. Fowkes, Attractive forces at interfaces, Ind. Eng. Chem. 56 (12) (1964) 40–52.
[30] P. Saffman, The lift on a small sphere in a slow shear flow, J. Fluid Mech. 22 (1965) 385 (and Corrigendum 31 (1968) pp. 624).
[31] J.G.A. Bitter, A study of erosion phenomena (Part II), Wear 6 (1963) 169–190.
[32] D. Bouris, G. Bergeles, Particle–surface interactions in heat exchanger fouling, J. Fluids Eng. 118 (1996) 574–581.
[33] J. Cleaver, B. Yates, Mechanism of detachment of colloidal particles from a flat substrate in a turbulent flow, J. Colloid Interface Sci. 44 (3) (1973) 464–474.
[34] S. Balabani, M. Yianneskis, An experimental study of the mean flow and turbulence structure of cross-flow over tube bundles, Proc. Inst. Mech. Eng., Part C: Mech. Eng. Sci. 210 (1996) 317–331.
[35] E. Konstantinidis, D. Castiglia, S. Balabani, M. Yianneskis, On the velocity and vortex shedding characteristics of an in-line tube bundle in steady and pulsating cross-flow, Chem. Eng. Res. Des, Trans. IChemE, Part A 78 (A8) (2000) 1129–1138.
[36] D. Castiglia, Fluid flow and heat transfer in unconventional tube bundle arrangements in crossflow, Ph.D. thesis, King's College London, University of London, 2002.
[37] S. Balabani, An experimental investigation of the crossflow over tube bundles, Ph.D. thesis, King's College London, University of London, 1996.
[38] S. Balachandar, R. Mittal, F.M. Najjar, Properties of the mean recirculation region in the wakes of two-dimensional bluff bodies, J Fluid Mech. 351 (1997) 167–199.
[39] Y. Nakamura, Vortex shedding from bluff bodies and a universal Strouhal number, J. Fluids Struct. 10 (1996) 159–171.
[40] P. Tochon, J.M. Grillot, in: G. Bergeles, M. Yianneskis, J.M. Grillot, N. Giannopoulos, S. Balabani, D. Bouris, D. Castiglia, E. Konstantinidis, G. Papadakis, P. Tochon (Eds.), Fouling minimisation and process intensification in heat exchangers of lignite utility boilers. Publishable Report, JOE3-CT97-0064, JOULE III Non Nuclear Energy Programme, European Commission, 2000.